The role of Ln^{3+} (Ln = Eu, Yb) in persistent red luminescence in $MgGeO_3:Mn^{2+}$

Katayama, Y.; Kayumi, T.; Ueda, J.; Dorenbos, Pieter; Viana, B; Tanabe, S

DOI
10.1039/C7TC03151C

Publication date
2017

Document Version
Accepted author manuscript

Published in
Journal of Materials Chemistry C: materials for optical and electronic devices

Accepted Author Manuscript of http://dx.doi.org/10.1039/C7TC03151C

Journal Name

ARTICLE

Role of Ln^{3+} (Ln=Eu, Yb) on persistent red luminescence in $MgGeO_3$: Mn^{2+}

Received 00th January 20xx,
Accepted 00th January 20xx

DOI: 10.1039/x0xx00000x

www.rsc.org/

Y. Katayama,[a,b†] T. Kayumi,[a†] J. Ueda,[a] P. Dorenbos,[c] B. Viana[d] and S. Tanabe[a]

In this paper, Mn^{2+} and Ln^{3+} (Ln = Eu, Yb) co-doped $MgGeO_3$ phosphors were prepared by a solid state reaction technique, and their optical properties were investigated. Mn^{2+}-doped samples exhibit persistent luminescence in the red region, peaking at 677 nm, because of the $^4T_1 \rightarrow {}^6A_1$ transition of the Mn^{2+} ions under ultraviolet (UV) excitation. Based on the charge transfer (CT) transition of Eu^{3+} and the band-gap energy, energy level diagrams with divalent lanthanide ground states relative to the conduction and valence band edges were constructed. ΔE(Ln), (Ln = Eu, Yb), which represents the energy gaps between the divalent lanthanide ground states and the bottom of the conduction band, were found to be 0.95 and 0.52 eV, respectively. Compared to a Mn^{2+} singly- doped sample, the thermoluminescence (TL) glow curves of the Mn^{2+}-Eu^{3+} co-doped sample and the Mn^{2+}-Yb^{3+} co-doped sample showed an additional TL glow peak at approximately 502 and 332 K with trap depths (E_{trap}) of 1.49 and 0.99 eV, respectively. The correspondence of E_{trap} with ΔE(Ln) suggests that Eu^{3+} and Yb^{3+} themselves work as electron traps in the $MgGeO_3$: Mn^{2+} phosphors. We have also demonstrated that the Mn^{2+}-Eu^{3+} co-doped material could be a good probe with photo-stimulated functions for long-term *in vivo* imaging owing to its deeper trap depth.

Introduction

After the discovery of the green emitting $SrAl_2O_4$:Eu^{2+}-Dy^{3+} phosphor in 1996 by Matsuzawa *et al.*[1], many visible persistent phosphors have been developed for night lighting, safety signs, and related applications[3-5].

Recently, red to near-infrared (NIR) persistent phosphors have attracted considerable attention because of their potential applications for *in vivo* imaging[6]. The advantages of using red-to-NIR persistent phosphor for *in vivo* imaging in comparison with the other fluorescent probes can be summarised as follows. Red-to-NIR luminescence corresponds to the spectral range that has high transmittance through biological tissues[7]. Excitation before injection reduces photo-toxicity on biological tissues[6] and leads to a higher signal-to-noise ratio because of the extinction of scattering of excitation light and the absence of the autofluorescence of biological tissues[8]. To date, many red-to-NIR persistent phosphors activated with Eu^{2+}, Mn^{2+} and Cr^{3+} ions[1, 6, 9-17] have been reported because the transition wavelength is suitable for *in vivo* application in the so-called first biological window[18].

Mn^{2+}-activated phosphors show, depending on the crystal field strength, various luminescence colours, from blue-green to deep-red, that arises from 3d-3d intra-atomic transitions (Mn^{2+}:$^4T_1 \rightarrow {}^6A_1$) in inorganic materials. Generally, red luminescence, which is suitable for *in vivo* application, is achieved when Mn^{2+} ions are in octahedral coordination sites[6, 10, 11]. In the $MgGeO_3$ enstatite host, one of the pyroxene structures with two kinds of six-fold Mg and fourfold Ge sites, Mn^{2+} shows red luminescence at 680 nm owing to the incorporation of Mn into Mg sites. In 2003, Iwasaki *et al.* investigated the effect of lanthanide co-doping on the persistent luminescence of $MgGeO_3$:Mn^{2+} and reported that, among the fourteen lanthanide ions, only Yb co-doping increases the persistent luminescence intensity of $MgGeO_3$:Mn^{2+}[19]. They proposed that Yb^{3+} may be a natural electron trap and that trivalent and divalent are both possible states. However, it is still unclear why in the $MgGeO_3$ host, only Yb^{3+} acts as a good co-dopant to enhance the persistent luminescence.

Persistent luminescence occurs when a material has two types of defects, one serving as a recombination and luminescence centre and the other as a carrier trap centre. Both need to have the ground state level located in the forbidden gap. As mentioned above, the introduction of an

[a] Graduate School of Global Environmental Studies, Kyoto University, 606-8501 Kyoto, Japan.
[b] Graduate School of Arts and Sciences, The University of Tokyo, 153-8902 Tokyo, Japan. Tel: 81 3 5454 6559; E-mail: katayama@phys.c.u-tokyo.ac.jp
[c] Faculty of Applied Sciences, Luminescence Materials Research group (FAME-LMR), Department of Radiation Science and Technology, Delft University of Technology, 2629 JB Delft, The Netherlands.
[d] Institut de Recherche de Chimie-Paris, CNRS - Chimie-ParisTech, 75231 Paris Cedex 05, France
† Y. Katayama and T. Kayumi contributed equally to this work, which was done in Kyoto University.
Electronic Supplementary Information (ESI) available: Photoluminescence, photoluminescence excitation, and thermoluminescence spectra and initial rise plot of thermoluminescence glow curve of MGO:Mn^{2+}-Yb^{3+} were shown. See DOI: 10.1039/x0xx00000x [a]

appropriate defect level as a trap centre is often achieved by co-doping with lanthanide ions[2,3,19]. Recently, a helpful tool to discuss the trap depth generated by lanthanide co-doping has been established by Dorenbos[20-23]. This model is semi-empirical and offers information on the energy relationship between the valence and conduction (VB, CB) band edges and ground states of divalent and trivalent lanthanide ions. For instance, the carrier trapping properties of YPO_4 doped with Ce^{3+}/Pr^{3+} and Ln^{3+} (Ln=Nd, Er, Ho, Dy) have been modelled, following Dorenbos, an electron trapping model with Ln co-dopants, where Ce^{3+}/Pr^{3+} are the hole trapping recombination centres[24, 25].

In this paper, we applied the Dorenbos model to $MgGeO_3$:Mn^{2+}-Ln^{3+} (Ln = Eu and Yb) red persistent phosphors and investigated their persistent luminescence properties. We found that next to Yb, only Eu can work as an electron trap in the $MgGeO_3$:Mn^{2+} phosphor and demonstrated that $MgGeO_3$:Mn^{2+}-Eu^{3+}, which provides a deeper trap than Yb^{3+}, works as a storage phosphor.

Experimental procedures

Samples preparation

Polycrystalline ceramics with compositions of $Mg_{0.997}Mn_{0.002}Yb_{0.001}GeO_3$ and $Mg_{0.9977}Mn_{0.002}Eu_{0.0003}GeO_3$ were prepared by a solid-state reaction. The chemical reagents, MgO (4N), GeO_2 (4N), $MnCO_3$ (5N), Eu_2O_3 (4N), and Yb_2O_3 (4N) were used as starting materials. MgO was fired at 1300 °C for 13 h for dehydration and decarbonisation before weighing, because it reacts with H_2O and CO_2 in the air to some extent. Batches of the starting materials were mixed in the presence of ethanol. After drying, the mixture was sintered at 1200 °C for 5 h in air. The batches were ground in an alumina mortar to form homogeneous fine powder mixtures. Pellets of 13-mm diameter were sintered at 1300 °C for 2 h. As references, non-doped, Mn^{2+} singly-doped, Eu^{3+} singly doped, and Yb^{3+} singly doped polycrystalline ceramics with compositions of $MgGeO_3$ (MGO), $Mg_{0.998}Mn_{0.002}GeO_3$, $Mg_{0.9997}Eu_{0.0003}GeO_3$, and $Mg_{0.999}Yb_{0.001}GeO_3$ were also synthesised by the same method. The Eu containing samples were sintered in oxidising atmosphere. A cation ratio [Ge]/(all cations except [Ge]) of 1.05 was adopted to avoid the generation of the Mg-rich impurity phase, Mg_2GeO_4, because of the volatile nature of GeO_2 above 1250 °C. The $ZnGa_2O_4$:Cr^{3+} phosphor with composition of $Zn_{0.98}(Ga_{0.995}Cr_{0.005})_2O_4$ was used as a reference for the persistent luminescence decay curve[1] measurements. Sample names, compositions and sintering atmospheres of all the prepared samples are listed in Table 1.

Characterization

The crystalline phases of the obtained samples were identified by powder X-ray diffraction (Rigaku, Ultima IV). Diffuse reflectance spectra were measured using a scanning-type spectrophotometer (Shimadzu, UV3600) with a $BaSO_4$-based integrating sphere. Photoluminescence excitation (PLE) spectra were measured using a fluorescence spectrophotometer (Shimadzu, RF-5300). The persistent luminescence decay curves were recorded using a photomultiplier (Hamamatsu, R928) after the samples had been irradiated by a 300-W xenon lamp (Asahi Spectra, Max 302) with a UV mirror module (250 to 380 nm) for 5 min. Then, the afterglow intensity was converted into an absolute intensity (radiance, in units of $mW \cdot sr^{-1} \cdot m^{-2}$) by using a calibrated charge-coupled device (CCD) spectrometer (B&W Tek, Glacier X). Photoluminescence (PL) spectra and persistent luminescence spectra were measured using a CCD spectrometer (Ocean Optics, QE65pro). All PL and persistent luminescence spectra were corrected for the detector response using a standard halogen lamp (Labsphere SCL-600). Thermoluminescence (TL) glow curves of the red Mn^{2+} luminescence were recorded using the photomultiplier. A band-pass filter (380 to 700 nm) and a long-pass filter (600 nm) were fixed in front of the photomultiplier to cut off the noise. The samples were first cooled to 100 K and exposed to the same xenon lamp with the UV module for 10 min. After another 10 min of waiting time, the samples were heated to 600 K. The temperature dependence of the PL spectra of the MGO:Mn^{2+}-Eu^{3+} and MGO:Mn^{2+}-Eu^{3+} samples were measured under 290-nm excitation, which was obtained by a combination of a band-pass filter and the xenon lamp. In the photostimulated luminescence (PSL) measurements, the samples were kept at 37 °C (living body temperature), for 11 days after UV irradiation for 5 min. Subsequently, the PSL decay curves were detected with the photomultiplier under repeating on and off cycle of a 977-nm laser diode (LD) (Lumics, LU0977M300) every 5 min.

Results and discussion

Incorporation of lanthanide ions into the $MgGeO_3$ lattice

Figure 1 shows the X-ray diffraction patterns of all the obtained $MgGeO_3$ samples. For all the samples, $MgGeO_3$ with orthorhombic enstatite structure was obtained as a single phase(ICDD No.01-084-0768). No shift in the diffraction peaks was observed in these samples with different dopants.

Because the ionic radius of Ge^{4+} (0.39 Å) in four-fold coordination is too small for Mn^{2+}, Eu^{3+} and Yb^{3+} dopants, whose radii in six-fold coordination site are 0.67, 0.95, and 0.87 Å, respectively, are very likely incorporated into Mg^{2+} six-fold sites (0.72 Å)[26]. Based on the XRD results, no impurity phases were present in any sample (Figure 1). This result suggests that larger lanthanide ions, Eu and Yb, as well as Mn ions, are incorporated into the $MgGeO_3$ lattice.

Table 1, Nominal compositions and applied sintering atmospheres of samples.

Notation	Composition	Atmosphere
MGO	$MgGeO_3$	Air
MGO:Mn^{2+}	$Mg_{0.998}Mn_{0.002}GeO_3$	Air
MGO:Eu^{3+}	$Mg_{0.9997}Eu_{0.0003}GeO_3$	O_2
MGO:Yb^{3+}	$Mg_{0.999}Yb_{0.001}GeO_3$	Air
MGO:Mn^{2+}-Eu^{3+}	$Mg_{0.9977}Mn_{0.002}Eu_{0.0003}GeO_3$	O_2
MGO:Mn^{2+}-Yb^{3+}	$Mg_{0.997}Mn_{0.002}Yb_{0.001}GeO_3$	Air
ZGO:Cr^{3+}	$Zn_{0.98}(Ga_{0.995}Cr_{0.005})_2O_{3.98}$	Air[1]

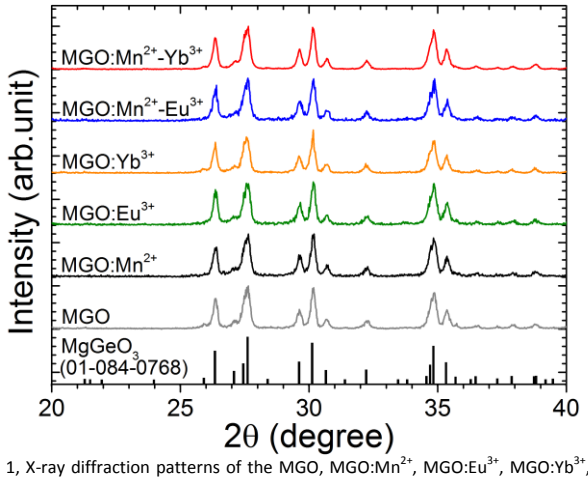

Fig. 1, X-ray diffraction patterns of the MGO, MGO:Mn^{2+}, MGO:Eu^{3+}, MGO:Yb^{3+}, MGO:Mn^{2+}-Eu^{3+} and MGO:Mn^{2+}-Yb^{3+} samples.

PL and persistent luminescence properties

Figure 2 shows the normalised PL and persistent luminescence spectra of the MGO:Mn^{2+}-Yb^{3+} under and after 290-nm excitation. The intensity in the range of 900–1040 nm is enlarged tenfold. In the PL spectrum, a red luminescence band peaking at 677 nm because of the Mn^{2+}:$^4T_1 \rightarrow {}^6A_1$ transition is observed together with sharp lines near 1000 nm arising from the Yb^{3+}:$^2F_{5/2} \rightarrow {}^2F_{7/2}$ transitions. The persistent luminescence spectrum is mainly composed of the red luminescence band due to Mn^{2+} and only very weak luminescence lines of Yb^{3+} can be observed. Although we do not discuss this in detail in this paper, this result indicates that the mechanisms of Yb^{3+} luminescence in PL and persistent luminescence are different[27].

In the PL spectrum of MGO:Mn^{2+}-Eu^{3+}, the same Mn^{2+} luminescence band was observed together with low-intensity peaks due to Eu^{3+}:$^5D_0 \rightarrow {}^7F_J$ transitions (see Figure S1).

Figure 3 shows the persistent luminescence decay curves of the MGO:Mn^{2+}, MGO:Mn^{2+}-Eu^{3+}, MGO:Mn^{2+}-Yb^{3+}, and $ZnGa_2O_4$:Cr^{3+}(ZGO:Cr^{3+}) phosphors after 5 min of UV irradiation. One hour after ceasing the UV excitation, the radiance intensities of the MGO:Mn^{2+}, MGO:Mn^{2+}-Eu^{3+}, MGO:Mn^{2+}-Yb^{3+} , and ZGO:Cr^{3+} samples were found to be 2.9×10^{-3}, 4.3×10^{-3}, 7.8×10^{-2} and 1.5×10^{-2} mW·sr^{-1}·m^{-2}, respectively. It was found that co-doping of both Eu^{3+} and Yb^{3+} increases the persistent luminescence intensity. In particular, that of MGO:Mn^{2+}-Yb^{3+} was approximately 27 times stronger than that of MGO:Mn^{2+} and 5 times larger than that of ZGO:Cr^{3+}, which is currently the most promising candidate persistent phosphor for *in vivo* imaging applications[8, 12]. Enhancement of the persistent luminescence intensity by Yb^{3+} co-doping in the $MgGeO_3$:Mn^{2+} phosphor, reported in 2003[19] was confirmed with quantitative values in radiance units.

To obtain information on the trap depth, TL glow curve measurements were performed. The TL glow curves monitoring the Mn^{2+} red luminescence of MGO:Mn^{2+}, MGO:Mn^{2+}-Eu^{3+}, and MGO:Mn^{2+}-Yb^{3+} samples are shown in the upper figure of Figure 4. The spectrum of MGO:Mn^{2+} contains several glow peaks at approximately 150, 400, and 450 K. The TL glow curves of MGO:Mn^{2+}-Eu^{3+} and MGO:Mn^{2+}-Yb^{3+} contain intense additional peaks at approximately 480 and 320 K, respectively. The peak temperature at 320 K of MGO:Mn^{2+}-Yb^{3+} is regarded as the most useful glow temperature for an excellent persistent phosphor. To estimate the trap depth from the TL glow curves, the thermal quenching properties were examined from the temperature dependence of the integrated PL intensity of Mn^{2+} transitions in MGO:Mn^{2+}-Eu^{3+} and MGO:Mn^{2+}-Eu^{3+} (see Figure. 4 lower graph). The PL intensity first increased with temperature up to 300 K for MGO:Mn^{2+}-Eu^{3+} and 400 K for MGO:Mn^{2+}-Yb^{3+}, which is probably due to the thermal release of a trapped electron from the defects. Both MGO:Mn^{2+}-Eu^{3+} and MGO:Mn^{2+}-Yb^{3+} samples showed quenching above 400 K. The TL glow peak at 480 K in the raw data of the MGO:Mn^{2+}-Eu^{3+} sample is affected by thermal quenching. Thermal quenching curves were fitted by using a single barrier quenching function[28].

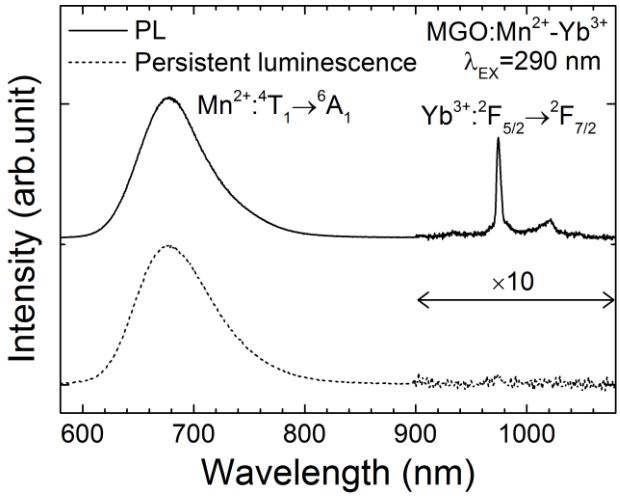

Fig.2 PL spectrum by 290 nm excitation (solid) and persistent luminescence spectrum (dashed) 10 s after ceasing the excitation light of MGO:Mn^{2+}-Yb^{3+}.

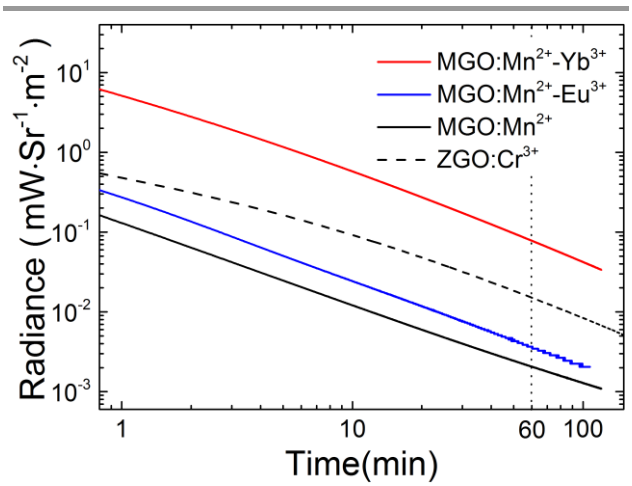

Fig.3 Persistent luminescence decay curves of MGO:Mn^{2+}, MGO:Mn^{2+}-Eu^{3+}, MGO:Mn^{2+}-Yb^{3+} and ZGO:Cr^{3+} phosphors after 5 min of UV irradiation.

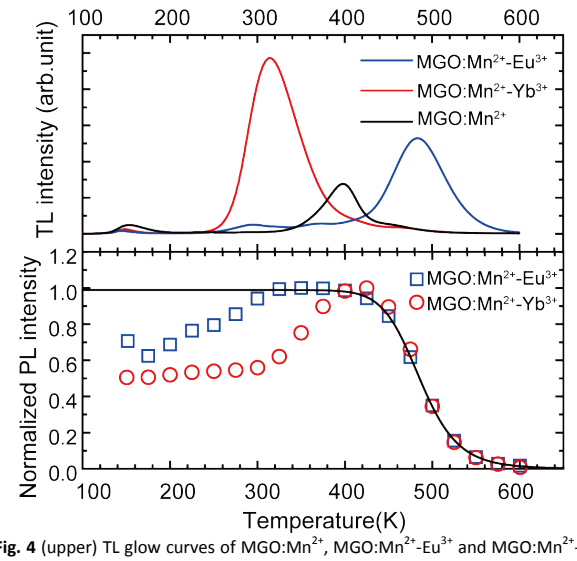

Fig. 4 (upper) TL glow curves of MGO:Mn^{2+}, MGO:Mn^{2+}-Eu^{3+} and MGO:Mn^{2+}-Yb^{3+} with heating rate of 10 K/min. A Xe lamp UV light source was used for storage for 10 min at 100 K. (bottom) Steady state temperature dependence of PL integrated intensity in the range 550-900 nm (Mn^{2+} luminescence band) of MGO:Mn^{2+}-Eu^{3+} and MGO:Mn^{2+}-Yb^{3+} samples by 290 nm excitation. Black line represents fitted curves for MGO:Mn^{2+}-Eu^{3+} by Eq.1.

$$\frac{I(T)}{I_0} = \frac{1}{1+\Gamma_o/\Gamma_v \exp(-E_q/kT)} \qquad (1)$$

Here, I is the luminescence intensity, Γ_v is the radiative decay rate, Γ_0 is the attempt rate of the nonradiative process, E_q is the activation energy, k is the Boltzmann constant, and T is the temperature. The fitted parameters are summarised in Table 2. Three parameters, $T_{50\%}$, Eq and Γ_0/Γ_v, were 486 K, ~1 eV, and ~10^{10} s^{-1}, respectively, and these values estimated from the two samples are in good agreement within the uncertainty. Because the radiative decay rate (Γ_v) of Mn^{2+} in oxide materials[29] is ~10^3 s^{-1}, Γ_0 is on the order of ~$10^{13}$$s^{-1}$, which is a similar magnitude to that of the maximum phonon frequency in oxide compounds. By correcting TL glow curve, the TL peak temperatures of 335 K and 502 K were obtained for MGO:Mn^{2+}-Eu^{3+} and MGO:Mn^{2+}-Yb^{3+} samples, respectively (see Table 3).

Trap depths were estimated using the first-order kinetics recombination model, which satisfies Eq.2.

$$\frac{\beta E_{trap}}{kT_m^2} = s\exp\left(-\frac{E_{trap}}{kT_m}\right) \qquad (2)$$

Here, β is the heating rate, E_{trap} is the trap depth, k is the Boltzmann constant, T_m is the peak temperature of the TL glow curve, and s is frequency factor[30]. A value of 1 × 10^{13} s^{-1} was used as a frequency factor, which is considered constant and is on the order of the lattice vibration frequency[31]. Estimated trap depths (E_{trap}) were 1.49 eV for MGO:Mn^{2+}-Eu^{3+} and 0.99 eV for MGO:Mn^{2+}-Yb^{3+} (as listed in Table 2). By adopting a thermal cleaning method for MGO:Mn^{2+}-Yb^{3+} sample at 230 K, we obtained a value of 0.83 eV, which represents the shallowest trap depth of the peak (the initial rise plot for the TL is shown in Figure. S4).

Figure 5 shows wavelength–temperature contour plots of the wavelength-resolved TL measurement performed on (a) MGO:Mn^{2+}-Eu^{3+} and (b) MGO:Mn^{2+}-Yb^{3+}. In both samples, the TL spectra mainly consist of the 680-nm red Mn^{2+} luminescence band. In the case of MGO:Mn^{2+}-Yb^{3+}, a TL emission of Yb^{3+}, peaking at approximately 980 nm, is also seen, while the Eu^{3+} emission in MGO:Mn^{2+}-Eu^{3+} was not observed (see Figure S3, TL spectra for both samples at the TL glow maxima, horizontal cross-sections of Figure 5).

Construction of the energy level diagram of $MgGeO_3$:Ln

To obtain the energy difference between the divalent lanthanide ground states and the band-edges of $MgGeO_3$, the bandgap energy and the charge transfer (CT) energy of Eu^{3+} were determined. Figure 6 shows the diffuse reflectance spectrum and the Tauc plot of the MGO sample. MGO has an the absorption edge at approximately 220 nm. The optical bandgap energy was determined as follows. First, the measured diffuse reflectance, R, was converted into a Kubelka-Munk function, $F(R)$[32] (Eq. 3), which is proportional to the absorption coefficient K if the scattering coefficient S is independent of wavelength.

$$F(R) \equiv \frac{K}{S} = \frac{(1-R)^2}{2R} \qquad (3)$$

As an approximation, the scattering coefficient S was treated as a constant.

Then, the optical bandgap energy (E_g) was determined from a Tauc plot[33] (Eq. 4) using the Kubelka-Munk function.

$$(h\nu F(R))^2 = A(h\nu - E_g) \qquad (4)$$

Here, $h\nu$ is the photon energy, and A is a constant. From the Tauc plot, the bandgap energy at ambient temperature was calculated to be 5.68 eV from the x-section of the tangent to the curve, as shown in Figure 6 (inset).

Table 2. Quenching temperature ($T_{50\%}$), activation energy of quenching (Eq), ratio of attempt rate, and radiative rate (Γ_0/Γ_v), from the luminescence quenching curves.

Sample name	$T_{50\%}$	E_q (eV)	Γ_0/Γ_v,(s^{-1})
MGO:Mn^{2+}-Eu^{3+}	486	0.93(3)	$5(3) \times 10^9$
MGO:Mn^{2+}-Yb^{3+}	486	1.05(9)	$8(2) \times 10^{10}$

Table 3. TL peak temperature (T_m), estimated trap depth (E_{trap}), and the energy gap between the bottom of the conduction band and the ground states of divalent lanthanide (ΔE) in the $MgGeO_3$ lattice.

Lanthanide	T_m (K)	E_{trap} (eV)	ΔE (eV)
Eu	502	1.49	0.95
Yb	335	0.99	0.52

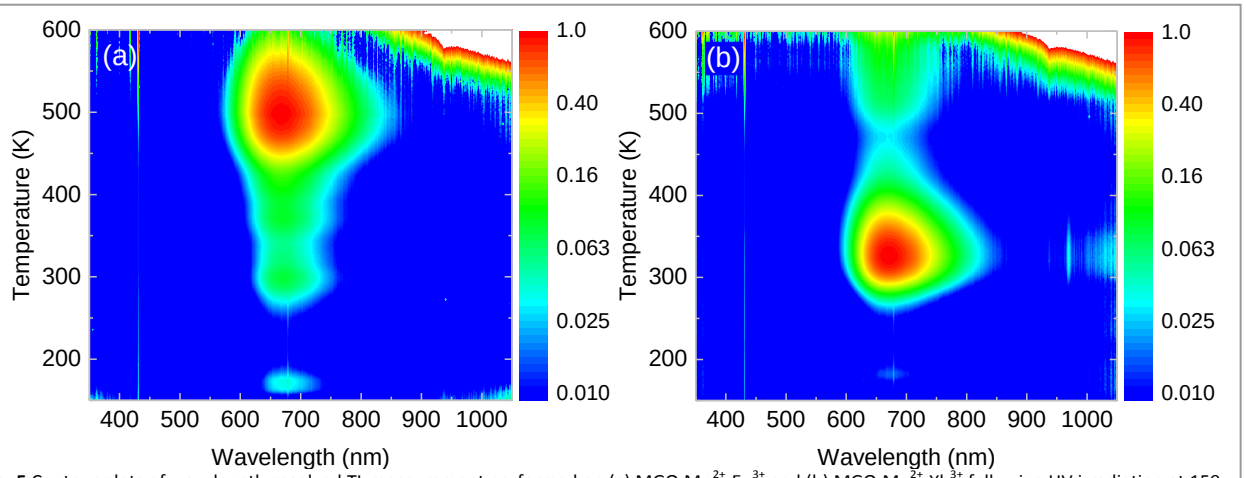

Fig. **5** Contour plots of wavelength-resolved TL measurement performed on (a) MGO:Mn^{2+}-Eu^{3+} and (b) MGO:Mn^{2+}-Yb^{3+} following UV irradiation at 150 K at a heating rate at 10 K/min. Colour distribution explanation: The intensity is presented in false colours. The top right intensity for the highest temperature is related to the blackbody radiation.

Figure 7 shows the PLE spectrum of MGO: Eu^{3+} monitoring the Eu^{3+}: $^5D_0 \rightarrow {}^7F_2$ transition at 621 nm. The PLE spectrum shows a broad band peaking at 262 nm (4.73 eV) with several $4f^6$-$4f^6$ excitation lines in the range of 320–470 nm. The broad band is attributed to the electron transfer from the top of the VB to Eu^{3+} with the ground state of Eu^{2+} as its final state[21]. Based on these results, an energy level diagram that shows the relative energy locations of the band-edge and the ground states of divalent lanthanide ions was constructed, as shown in Figure 8. The ground state energy of Eu^{2+} was defined as the zero of energy. The vertical axis then represents the Eu^{2+} referred electron binding energy (ERBE). From the CT energy of Eu^{3+} (E_{CT}), the top of the VB is 4.73 eV below the ground state of Eu^{2+}. According to Dorenbos theory, the 4f electron ground state binding energies of the divalent lanthanides follow a zigzag curve that remains practically unchanged through all oxide materials[20, 21]. Figure 8 shows that only the ground states for Eu^{2+} and Yb^{2+} lie below the bottom of the CB. This implies that of the fourteen lanthanide ions only Eu^{3+} and Yb^{3+} ions act as electron traps in the $MgGeO_3$ host. Because the optical bandgap energy of $MgGeO_3$ is 5.68 eV, the energy gaps between the ground state of the Ln^{2+} (Eu and Yb) ions and the bottom of the CB, ΔE were found to be 0.95 and 0.52 eV from the simple subtraction of E_{CT} from E_g (see Figure 8).

Here, we should mention that the optical bandgap was used for the construction of the energy level diagram. Based on the Dorenbos model[34], the mobility bandgap is estimated from the energy of host exciton creation at a low temperature (10 K). However, the exciton binding energy, estimated as 8 % of the exciton creation energy, is required to reach the CB bottom. From the PLE spectrum monitoring the Mn^{2+} luminescence at room temperature, a host-related band, peaking at 210 nm, was observed in MGO:Mn^{2+} (Figure S2). This would suggest that the mobility band edge is located near 6.4 eV at room temperature.

Persistent luminescence mechanism in $MgGeO_3$:Mn^{2+}-Ln^{3+} (Ln = Eu, Yb)

The estimated values of E_{trap} and ΔE for MGO:Mn^{2+}-Eu^{3+} are larger than those for MGO:Mn^{2+}-Yb^{3+}. For both Eu and Yb, E_{trap} is larger than ΔE (Table 3). Note that we have adopted the optical bandgap for the estimation of ΔE. When a bandgap of 6.4 eV, which is estimated according to the Dorenbos model, is

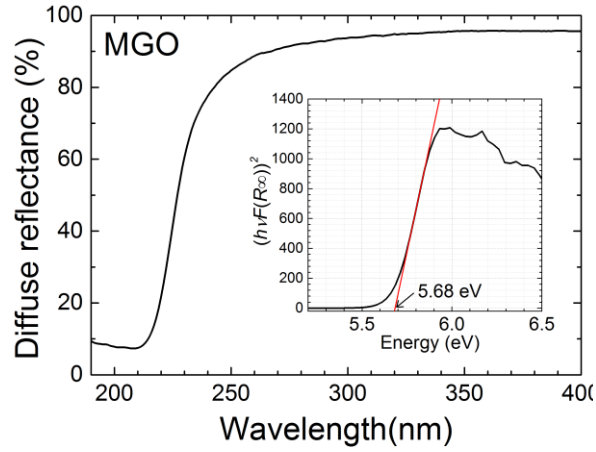

Fig..6 Diffuse reflectance spectrum and Tauc plot of the MGO sample.

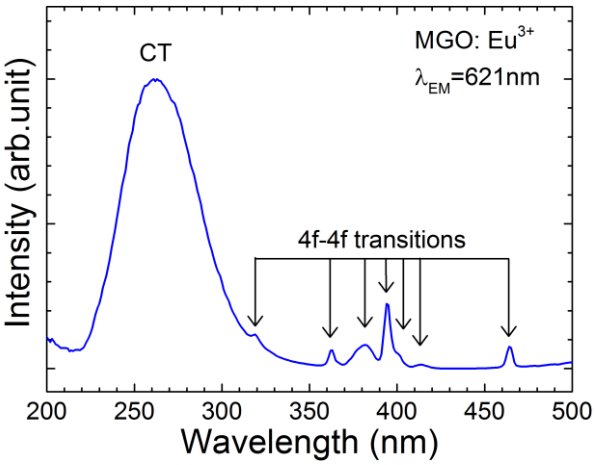

Fig.. 7 PLE spectrum of MGO:Eu^{3+} monitoring Eu^{3+} luminescence at 621 nm.

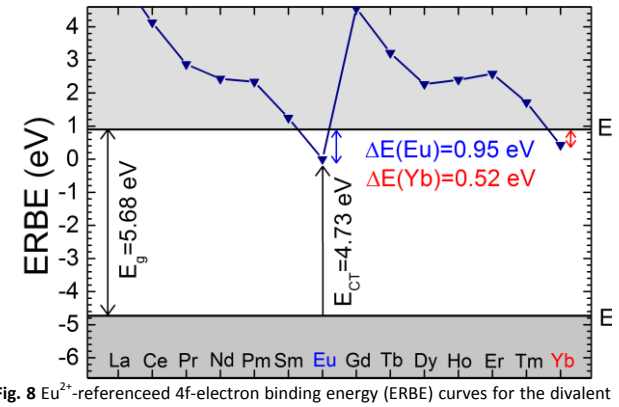

Fig. 8 Eu^{2+}-referenceed 4f-electron binding energy (ERBE) curves for the divalent lanthanide ions in $MgGeO_3$. E_{CB} and E_{VB} are the binding energies at the bottom of the conduction band and the top of the valence band.

adopted, *ΔE(Ln)* is in good agreement with E_{trap}*(Ln)*. In either case, the energy difference between *ΔE(Eu)* and *ΔE(Yb)* of 0.43 eV corresponds approximately to the ΔE_{trap} (= E_{trap}*(Eu)* – E_{trap}*(Yb)*) of 0.50 eV. There are many reasons why the trapping energy from the TL glow curve does not match well with that from the energy level scheme based on the Dorenbos model. In reports on the effect of *Ln* co-doping on Ce^{3+} and Pr^{3+} activated YPO_4 [24, 25], there were systematic differences of around 0.3-0.5 eV between the trap depth and the energy gap between the bottom of the CB and the ground state of a divalent lanthanide ion. They attributed such a difference to systematic uncertainty in the lanthanide levels in the Dorenbos diagram and to the different experimental approach between the construction of the energy level diagram (optical process) and estimation of the trap depth (thermally activated process) [21, 24, 25].

From the agreement between E_{trap} and *ΔE,* we conclude that Eu^{3+} and Yb^{3+} are good electron trapping centres in the $MgGeO_3$:Mn^{2+} phosphor noted as $Ln^{3+}+e^- \rightarrow Ln^{2+}$ (Ln^{3+}–e^-). It has been reported that persistent luminescence can be observed after 250-nm (4.96 eV) excitation, which corresponds to the CT band, $Mn^{2+} \rightarrow Mn^{3+}+e^-$ [19, 35]. The value of 4.96 eV is much smaller than the optical bandgap energy, 5.68 eV. Therefore, the persistent luminescence process in MGO:Mn^{2+}-Yb^{3+} is explained as follows. Under UV excitation at 250 nm, Mn^{2+} is photoionised and the electrons are trapped by Yb^{3+} or near Yb^{3+} to form Yb^{2+} ($Yb^{3+}+e^-$). After the light excitation, the trapped electrons are released from Yb^{2+} ($Yb^{3+}+e^-$) ions by thermal stimulation, and they recombine with the hole centre on Mn^{3+} producing the 680-nm red emission. In the case of MGO:Mn^{2+}-Eu^{3+}, persistent luminescence occurs because of non-Eu-related defects, which create the TL glow peak around room temperature seen in Figure 4(a). Thermal stimulation at room temperature is not sufficient to release the trapped electron from Eu^{2+} ($Eu^{3+}+e^-$), which provide a much deeper trap than Yb^{3+}. In other words, an electron trapped at Eu is stable at room temperature unless an athermal tunnelling detrapping process plays a major role. This suggests that MGO:Mn^{2+}-Eu^{3+} might work as a storage phosphor.

$MgGeO_3$:Mn^{2+}-Eu^{3+} as a storage phosphor for further applications in *in-vivo* imaging

NIR photo-stimulation of red-NIR persistent phosphors may have added-value for *in vivo* imaging[13, 36, 37]. By using a storage phosphor, one may obtain the signal several days after its injection into the body by means of NIR photo-stimulation.

To demonstrate the PSL output capacity, the following experiment was carried out. First, the MGO:Mn^{2+}-Yb^{3+} and MGO:Mn^{2+}-Eu^{3+} polycrystalline samples were irradiated with UV light from the Xe lamp for 5 min. Secondly, the temperature of the samples was kept at 37 °C in a furnace for 11 days. This temperature is the body temperature of some mammals, including humans. Finally, the red PSL signal was detected by a photomultiplier under 5 min 977-nm LD modulated square-wave photo-stimulation. These PSL reveal the deep traps in the materials.

Figure 9 shows the PSL decay curves of the red Mn^{2+} luminescence in MGO:Mn^{2+}-Yb^{3+} and MGO:Mn^{2+}-Eu^{3+}, which were obtained by the procedure explained above. Both MGO:Mn^{2+}- Yb^{3+} and MGO:Mn^{2+}-Eu^{3+} samples showed a PSL signal during the first 5 min photostimulation pulse. For MGO:Mn^{2+}-Eu^{3+}, the initial intensity of the PSL was approximately five times stronger than that of MGO:Mn^{2+}-Yb^{3+}. The PSL of MGO:Mn^{2+}-Eu^{3+} was detectable even after four photostimulation events (20 min total), while that of MGO:Mn^{2+}-Yb^{3+} was almost quenched during the first 5 min. Notice that the quenching speed of PSL depends on the LD intensity[35].

In the case of MGO:Mn^{2+}-Yb^{3+}, the TL glow peak was centred at 320 K with a tail extending at higher temperatures (see Figure 4). When the sample was kept at 37 °C (310 K) for 11 days, most of the trapped electrons were released by the thermally activated process. On the other hand, for MGO:Mn^{2+}-Eu^{3+}, the main TL peak was centred at 502 K with a higher thermal activation energy of 1.49 eV, and the electrons trapped at Eu^{3+} were maintained for 11 days. Thus, the PSL signal of MGO:Mn^{2+}-Eu^{3+} can be recorded several days and even more than one week after charging the material by UV

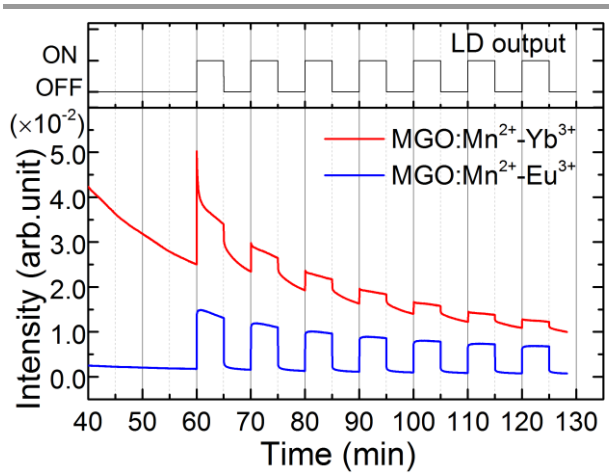

Fig.. 9 Photostimulated luminescence decay curves of red Mn^{2+} luminescence in MGO:Mn^{2+}-Eu^{3+} and MGO:Mn^{2+}-Yb^{3+} (lower) under 5 min square-wave pulsed photostimulation with a 97- nm LD (upper).

irradiation. This is a desirable feature for *in vivo* imaging applications. Indeed most cases of accumulation of optical sensors to target tumours of other diseases, enhanced permeability and retention (EPR) effect[39] require accumulation times exceeding several days. Here, we have demonstrated that PSL can undergo trap release after significantly extended periods post irradiation, and this could open the path to long-term imaging. Further investigation of the PSL process and in-detail measurement of the efficiency are required because the fading of the signal due to athermal tunnelling or another mechanism is possible.

Conclusions

The optical properties of Mn^{2+}-Ln^{3+} (Ln=Eu and Yb) co-doped $MgGeO_3$ ceramics were investigated to reveal the effect of trivalent lanthanide ions on the persistent luminescence properties. Based on the constructed energy diagram, the energy gaps (ΔE) between the bottom of the CB and the ground state of divalent lanthanides were estimated to be 0.95 eV for Eu and 0.52 eV for Yb, respectively. The lanthanide (Eu and Yb) co-doped $MgGeO_3$:Mn^{2+} showed an additional TL peak with trap depths, E_{trap}, at 1.49 and 0.99 eV, which were estimated from the TL results. It was suggested that Yb^{3+} and Eu^{3+} cations work well as an electron trap in the $MgGeO_3$ host and traps with Eu required more energy to realize in comparison with those creates with Yb, in good agreement with the stability of both divalent lanthanide cations.

MGO:Mn^{2+}-Yb^{3+} showed a five times larger persistent luminescence intensity than that of ZGO:Cr^{3+}, which is the primary candidate persistent phosphor for *in vivo* imaging. MGO:Mn^{2+}-Eu^{3+}, which has a deeper trap than MGO:Mn^{2+}-Yb^{3+}, showed PSL signal even after 11 days after UV irradiation, and, thus, may be a good probe with photostimulated functions for long-term *in-vivo* imaging. Consequently, $MgGeO_3$:Mn^{2+}-Ln^{3+} (Eu and Yb) red persistent phosphors are proven to be good candidates for *in vivo* imaging applications as persistent, in the case of Yb, and a storage, in the case of Eu cations, phosphors.

Acknowledgements

This work was financially supported by a Grant-in-Aid for Scientific Research for JSPS Fellows (NO. 26-40075).

Notes and references

1 T. Matsuzawa, Y. Aoki, N. Takeuchi and Y. Murayama, *J. Electrochem. Soc.*, 1996, 143, 2670-2673.
2 H. Yamamoto and T. Matsuzawa, *J. Lumin.*, 1997, 2313, 72-74.
3 X. Wang, Z. Zhang, Z. Tang and Y. Lin, *Mater. Chem. Phys.*, 2003, 80, 1-5.
4 J. Ueda, K. Kuroishi and S. Tanabe, *Appl. Phys. Lett.*, 2014, 104, 101904.
5 Q. le Masne de Chermont, C. Chanéac, J. Seguin, F. Pellé, S. Maîtrejean, J.-P. Jolivet, D. Gourier, M. Bessodes and D. Scherman, *P. Natl. Acad. Sci. USA.*, 2007, 104, 9266-9271.
6 R. Weissleder, *Nat. Biotechnol.*, 2001, 19, 316-317.
7 T. Maldiney, A. Bessière, J. Seguin, E. Teston, S. K. Sharma, B. Viana, A. J. J. Bos, P. Dorenbos, M. Bessodes, D. Gourier, D. Scherman and C. Richard, Nat. Mater., 2014, 13, 418-426.
8 T. Maldiney, G. Sraiki, B. Viana, D. Gourier, C. Richard, D. Scherman, M. Bessodes, K. V. d. Eeckhout, D. Poleman and P. F. Smet, *Opt. Mater. Express*, 2012, 2, 261-268.
9 A. Bessière, A. Lecointre, K. R. Priolkar and D. Gourier, *J. Mater. Chem.*, 2012, 22, 19039.
10 T. Maldiney, A. Lecointre, B. Viana, A. Bessière, M. Bessodes, D. Gourier, C. Richard and D. Scherman, *J. Am. Chem. Soc.*, 2011, 133, 11810-11815.
11 A. Bessière, S. Jacquart, K. Priolkar, A. Lecointre, B. Viana and D. Gourier, *Opt. Express*, 2011, 19, 10131-10137.
12 Y. Zhuang, J. Ueda and S. Tanabe, *Appl. Phys. Express*, 2013, 6, 052602.
13 F. Liu, W. Yan, Y.-J. Chuang, Z. Zhen, J. Xie and Z. Pan, *Sci. Rep.*, 2013, 3, 1554-1563.
14 Z. Pan, Y.-Y. Lu and F. Liu, *Nat. Mater.*, 2012, 11, 58-63.
15 M. Allix, S. Chenu, E. Véron, T. Poumeyrol, E. A. Kouadri-Boudjelthia, S. Alahraché, F. Porcher, D. Massiot and F. Fayon, *Chem. Mater.*, 2013, 25, 1600-1606.
16 D. Chen, Y. Chen, H. Lu and Z. Ji, *Inorg. Chem.*, 2014, 53, 8638-8645.
17 Y. Katayama, H. Kobayashi and S. Tanabe, *Appl. Phys. Express*, 2015, 8, 012102.
18 A. M. Smith, M. C. Mancini and S. Nie, *Nat. Nanotechnol.*, 2009, 4, 710-711.
19 M. Iwasaki, D. N. Kim, K. Tanaka, T. Murata and K. Morinaga, *Sci. Tech. Adv. Mater.*, 2003, 4, 137-142.
20 P. Dorenbos, *J. Phys.:Condens. Matter*, 2003, 15, 575-594.
21 P. Dorenbos, *J. Phys.:Condens. Matter*, 2003, 15, 8417-8434.
22 P. Dorenbos, *Phys. Rev. B*, 2012, 85, 165107.
23 P. Dorenbos, *J. Mater. Chem.*, 2012, 22, 22344.
24 A. Lecointre, A. Bessière, A. J. J. Bos, P. Dorenbos, B. Viana and S. Jacquart, *J. Phys. Chem. C*, 2011, 115, 4217-4227.
25 A. J. J. Bos, P. Dorenbos, A. Bessière and B. Viana, *Radiat. Meas.*, 2008, 43, 222-226.
26 R. Shannon, *Acta Crystallogr. Sect. A*, 1976, 32, 751-767.
27 Y.-j. Liang, F. Liu, Y.-f. Chen, X.-j. Wang, K.-n. Sun and Z. Pan, *Light Sci. Appl.*, 2016, 5, e16124.
28 P. Dorenbos, *J. Phys.:Condens. Matter*, 2005, 17, 8103-8111.
29 C. Barthou, J. Benoit, P. Benalloul and A. Morell, *J. Electrochem. Soc.*, 1994, 141, 524-528.
30 S. W. S. McKeever, *Thermoluminescence of solids*, Cambridge University Press, Cambridge, 1988.
31 A. J. J. Bos, *Radiat. Meas.*, 2006, 41, S45-S56.
32 S. Shionoya and W. M. Yen, *Phosphor Handbook*, CRC press, Boca Raton, 1998.
33 J. Tauc, R. Grigorovic and a. Vancu, *Phys. Status Solidi (B)*, 1966, 15, 627-637.
34 P. Dorenbos, *J. Lumin.*, 2005, 111, 89-104.
35 Y. Katayama, J. Ueda and S. Tanabe, *Opt. Mater. Express*, 2014, 4, 613-623.
36 Y. Zhuang, J. Ueda and S. Tanabe, *J. Phys. Chem. C*, 2013, 47, 2864-2869.
37 Y. Katayama, B. Viana, D. Gourier, J. Xu and S. Tanabe, *Opt. Mater. Express*, 2016, 6, 1405.
38 D. C. Rodríguez Burbano, S. K. Sharma, P. Dorenbos, B. Viana and J. A. Capobianco, *Adv. Opt. Mater.*, 2015, 3, 551-557.
39 Y. Matsumura and H. Maeda, *Cancer Res.*, 1986, 46, 6387-6392.

Supporting Information

Role of Ln^{3+} (Ln=Eu, Yb) on persistent red luminescence in $MgGeO_3$: Mn^{2+}

Yumiko Katayama*, Tomohiro Kayumi, Jumpei Ueda, Pieter Dorenbos, Bruno Viana and Setsuhisa Tanabe

*E-mail: katayama@phys.c.u-tokyo.ac.jp

Fig. S1 shows photoluminescence (PL) spectra of MGO:Mn^{2+}-Eu^{3+} and MGO:Mn^{2+}-Yb^{3+} under 290 nm excitation. The PL lines due to 4f-4f transitions of Ln^{3+}(Eu and Yb) ions were observed approximately at 620 nm (Eu^{3+}) and at 980 nm (Yb^{3+}). With increasing Yb concentration, The PL intensity of Mn^{2+} decreased and that of Yb^{3+} increased.

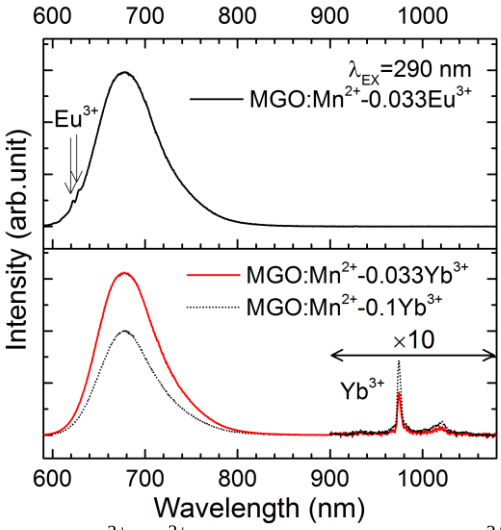

Fig. S1 PL spectra of MGO:Mn^{2+}-Eu^{3+} (upper) and MGO:Mn^{2+}-Yb^{3+} with different Yb concentration (lower) under 290 nm excitation. PL lines due to 4f-4f transitions of Ln^{3+}(Eu and Yb) ions were observed. With increasing Yb concentration, PL intensity of Mn^{2+} decreased and that of Yb^{3+} increased.

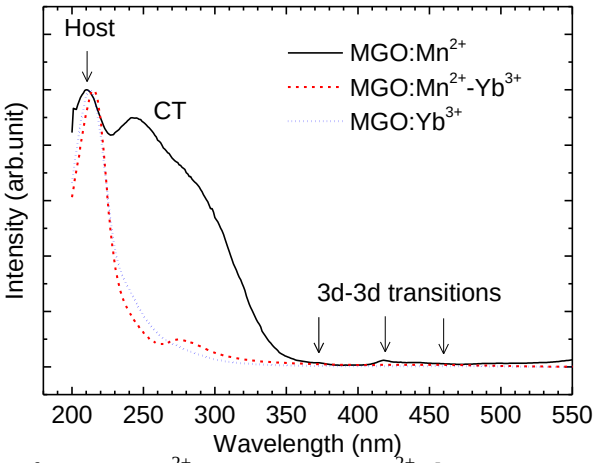

Fig. S2 PLE spectra of MGO:Mn^{2+} monitoring Mn^{2+} luminescence, MGO:Mn^{2+}-Yb^{3+} and MGO:Yb^{3+} samples monitoring Yb^{3+} luminescence.

The PLE spectra of the MGO:Mn^{2+}, MGO:Mn^{2+}-Yb^{3+}, and MGO:Yb^{3+} samples monitoring Mn^{2+} or Yb^{3+} luminescence are shown in Fig. S2. For all the spectra, host related PLE band was observed at 210 nm, as well as the bands due to the charge transfer at 250 nm and 3d-3d transitions of Mn^{2+}.

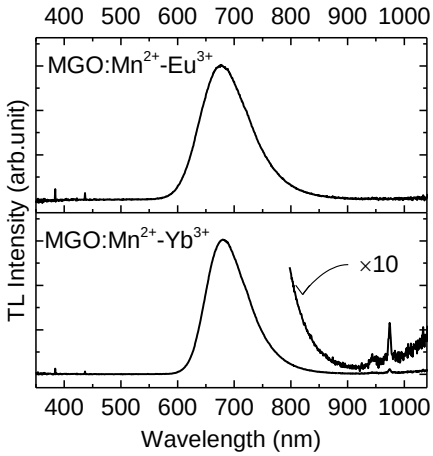

Fig. S3 TL spectra for MGO:Mn^{2+}-Eu^{3+} and MGO:Mn^{2+}-Yb^{3+} samples at the TL glow maxima, 496 K for MGO:Mn^{2+}-Eu^{3+} and 326 K for MGO:Mn^{2+}-Yb^{3+}. (a horizontal cross section in Fig.5).

Fig.S3 shows the TL spectra for MGO:Mn^{2+}-Eu^{3+} and MGO:Mn^{2+}-Yb^{3+} samples at the TL glow maxima. Both samples show a luminescence band peaking at 677 nm due to the Mn^{2+}. For the MGO:Mn^{2+}-Yb^{3+} sample, weak Yb^{3+} luminescence approximately at 1000 nm is also observed. The spectrum is similar to the persistent luminescence spectrum shown in Fig.2.

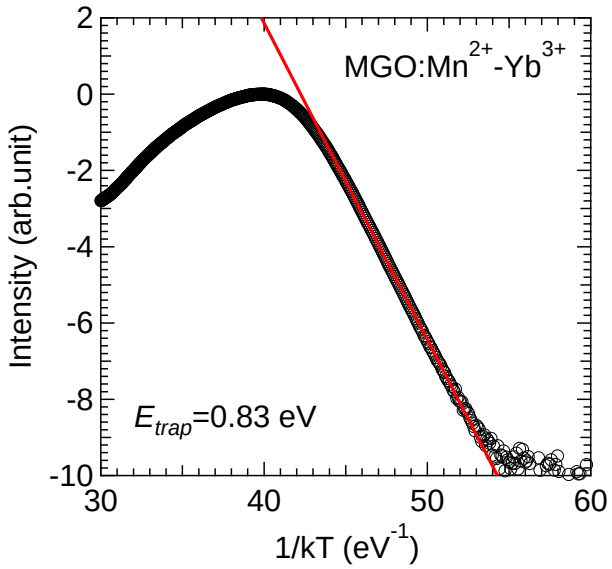

Fig.S4 Initial rise plot of the TL glow curve of MGO:Mn^{2+}-Yb^{3+} and corresponding fitted curve. TL was recorded by thermal cleaning method with thermal cleaning temperature at 230 K.

Fig.S4 shows initial rise plot of the TL glow curve of MGO:Mn^{2+}-Yb^{3+} recorded by thermal cleaning method. Trap depth was estimated by using a following equation.

$$I(T) \propto \mathrm{s} \cdot \exp\left(-\frac{E_{trap}}{kT}\right)$$

Here, s is a frequency factor, E_{trap} represents trap depth, k is Boltzmann constant and T is temperature. The estimated E_{trap} was 0.83 eV. When the trap depth distribution obeys Gaussian, trap depth created by Yb co-doping has an average value of 0.99 eV with 0.05-0.08 eV uncertainty.